

Long lifetime supersolid in a two-component dipolar Bose-Einstein condensate

Shaoxiong Li, Uyen Ngoc Le, and Hiroki Saito

Department of Engineering Science, University of Electro-Communications, Tokyo 182-8585, Japan

(Dated: March 22, 2022)

Recent studies on supersolidity in a single-component Bose-Einstein condensate (BEC) have relied on the Lee-Huang-Yang (LHY) correction for stabilization of self-bound droplets, which however involves a high density inside the droplets, limiting the lifetime of the supersolid. Here we propose a two-component mixture of dipolar and nondipolar BECs, such as an ^{166}Er - ^{87}Rb mixture, to create and stabilize a supersolid without the LHY correction, which can suppress the atomic loss and may allow observation of the long-time dynamics of the supersolid. In such a system, supersolidity can be controlled by the difference in the trap centers between the two components.

A supersolid state is a peculiar state of matter that possesses both the superfluidity of frictionless flow and the periodic spatial structure of a crystal. This counter-intuitive state of matter was originally predicted to arise in solid ^4He [1, 2]. However, such a state of matter was first realized in Bose-Einstein condensates (BECs) of ultracold atomic gases with a cavity-field interaction [3], spin-orbit interaction [4], and magnetic dipole-dipole interaction (DDI) [5–19]. In a BEC with a strong DDI, the matter wave splits into self-bound droplets, which form crystal structures [20]. Unlike incoherent isolated droplets simply placed in order, in a supersolid state, the matter-wave droplets allow superflow between them, giving rise to phase coherence. Due to the presence of a crystal structure with coherence, intriguing quantum properties emerge [21–35], such as a nonclassical moment of inertia [14] and low-energy Goldstone modes [8, 9].

In a self-bound droplet, the system is prone to collapse due to the attractive part of the DDI. The mean-field theory cannot explain the stability of the droplet against collapse [36, 37]. To explain the experimental observation of stable droplets the beyond-mean-field effect, called the Lee-Huang-Yang (LHY) correction [38], is needed. It was found that the Gross-Pitaevskii (GP) equation with the LHY correction can reproduce the experimental results quantitatively [39–42]. However, the LHY correction is a higher-order correction with respect to the atomic density, and in order to arrest the collapse, the density inside the droplet must be large. As a result, atomic loss due to three-body recombination becomes predominant, which limits the lifetime of the droplets [43, 44]. Thus, the lifetime of the supersolid is restricted as long as the LHY correction plays a dominant role in its stabilization. Moreover, the use of the Feshbach resonance also increases the atomic loss [44]. The limited lifetime of the supersolid hinders, for example, direct observation of the slow oscillation of Goldstone modes [9].

To circumvent this problem, in the present paper, we propose to use a two-component BEC. In a two-component BEC, there exist two kinds of excitation modes: density waves and quasi-spin waves. When the inter- and intra-component interactions are comparable to each other, the excitation energies of quasi-spin waves can be smaller than those of density waves. Consequently, the quasi-spin is more easily modulated than the

total density, and even a moderate strength of DDI can generate quasi-spin patterns without causing dipolar collapse. Two-component mixtures of dipolar BECs have been experimentally realized [45, 46] and theoretically investigated thoroughly [47–62]. A self-bound droplet including two components was also proposed [63, 64]. However, there have been few studies on supersolidity in two-component dipolar mixtures. Very recently, supersolid formation in a two-component dipolar BEC was theoretically studied [65]. However, in this study, the periodic structure is formed in the total density, not in the quasi-spin, and hence the LHY correction is needed to stabilize the droplets [65].

We use a ^{166}Er - ^{87}Rb mixture to study the two-component supersolid state. The magnetic moment of ^{166}Er is much larger than that of ^{87}Rb , and the ^{166}Er BEC forms droplets and a supersolid, while the ^{87}Rb BEC plays the role of a medium that accommodates them. The use of ^{166}Er is suitable for the present purpose, because the magnetic moment is not too large and the formation of LHY droplets can be avoided. Because of this moderate strength of DDI, for a single-component ^{166}Er BEC, reduction of the scattering length by Feshbach resonance is needed to produce the droplets [44]. By contrast, in our two-component system, we will show that the droplet lattice can be formed without reducing the scattering length, which also suppresses the atomic loss and prolongs the lifetime. We will show that one- and two-dimensional supersolid states can be formed, and that they are stabilized without the LHY correction. An important parameter in this system is the difference δ in the trap centers between the two components, including gravitational sag. By controlling δ , we can change the Josephson link between the droplets, and then we can control the degree of supersolidity. We will demonstrate that the long-period out-of-phase Goldstone mode appears when the supersolidity is enhanced by δ .

We employ the mean-field approximation at zero temperature to describe BECs of two atomic species with masses m_1 and m_2 and magnetic moments μ_1 and μ_2 . The magnetic moments of the atoms are fixed in the z direction by the magnetic field. The dynamics of the macroscopic wave functions $\psi_j(\mathbf{r}, t)$ can be described by

the coupled nonlocal GP equations [66] ($j = 1, 2$),

$$i\hbar \frac{\partial}{\partial t} \psi_j(\mathbf{r}, t) = \left[-\frac{\hbar^2}{2m_j} \nabla^2 + V_j(\mathbf{r}) + \sum_{j'=1}^2 g_{jj'} |\psi_{j'}(\mathbf{r}, t)|^2 + \frac{\mu_0 \mu_j}{4\pi} \int d\mathbf{r}' \frac{1 - 3 \cos^2 \theta}{|\mathbf{r} - \mathbf{r}'|^3} \sum_{j'=1}^2 \mu_{j'} |\psi_{j'}(\mathbf{r}', t)|^2 \right] \psi_j(\mathbf{r}, t), \quad (1)$$

where $g_{jj'} = 2\pi\hbar^2 a_{jj'}/m_{jj'}$ are the contact interaction coefficients, $a_{jj'}$ and $m_{jj'} = (m_j^{-1} + m_{j'}^{-1})^{-1}$ are the s -wave scattering lengths and the reduced masses between components j and j' , μ_0 is the magnetic permeability of the vacuum, and θ is the angle between $\mathbf{r} - \mathbf{r}'$ and the z direction. The wave functions are normalized as $\int d\mathbf{r} |\psi_j|^2 = N_j$, where N_j is the number of atoms in component j . We assume that the system is confined in an optical dipole trap with two different laser frequencies, by which the trap frequencies for the two components can be controlled individually. When the centers of the harmonic potentials for the two components horizontally coincide, the external potential can be written as

$$V_j(\mathbf{r}) = \frac{1}{2} m_j [\omega_{jx}^2 x^2 + \omega_{jy}^2 y^2 + \omega_{jz}^2 (z - \delta_j)^2], \quad (2)$$

where $\omega_{jx,y,z}$ are the trap frequencies for component j . The deviations of the trap centers δ_j in the z direction arise both from the gravitational sag and the laser alignment, which we simply call ‘‘sag’’ in the following. We define

$$\delta_1 - \delta_2 \equiv \delta. \quad (3)$$

We assume that components 1 and 2 consist of ^{166}Er atoms with $\mu = 7\mu_B$ and ^{87}Rb atoms with $\mu = \frac{1}{2}\mu_B$, respectively, where μ_B is the Bohr magneton. Such a two-component mixture with a large difference in magnetic moments is suitable for dipolar pattern formation. To understand this, for simplicity, suppose a uniform system with $g_{11} \simeq g_{22} \simeq g_{12}$. In this case, in the absence of the DDI, the total density $|\psi_1|^2 + |\psi_2|^2$ is almost constant (n), and we rewrite the contact interaction terms for component 1 in Eq. (1) as $(g_{11}|\psi_1|^2 + g_{12}|\psi_2|^2)\psi_1 = (g_{11} - g_{12})|\psi_1|^2\psi_1 + g_{12}n\psi_1$, which indicates that the effective interaction for component 1, i.e., that for quasi-spin, is $g_{11} - g_{12}$. Thus, the contact interaction is effectively reduced compared with the single-component system, and hence the relative strength of the DDI is increased. On the other hand, the dipolar interaction part can similarly be rewritten as $(\mu_1|\psi_1|^2 + \mu_2|\psi_2|^2)\psi_1 = (\mu_1 - \mu_2)|\psi_1|^2\psi_1 + \mu_2 n\psi_1$, and hence the effective magnetic moment for the quasi-spin is $\mu_1 - \mu_2$. This is the reason why we are using atomic species with $\mu_1 \gg \mu_2$. If $\mu_1 \simeq \mu_2$, the effective magnetic moment for the quasi-spin vanishes, and only total-density patterns appear, as in Ref. [65].

We numerically solve the three-dimensional GP equation (1) using the pseudospectral method. The spatial discretization is typically $dx = dy = dz \simeq 0.3 \mu\text{m}$ and

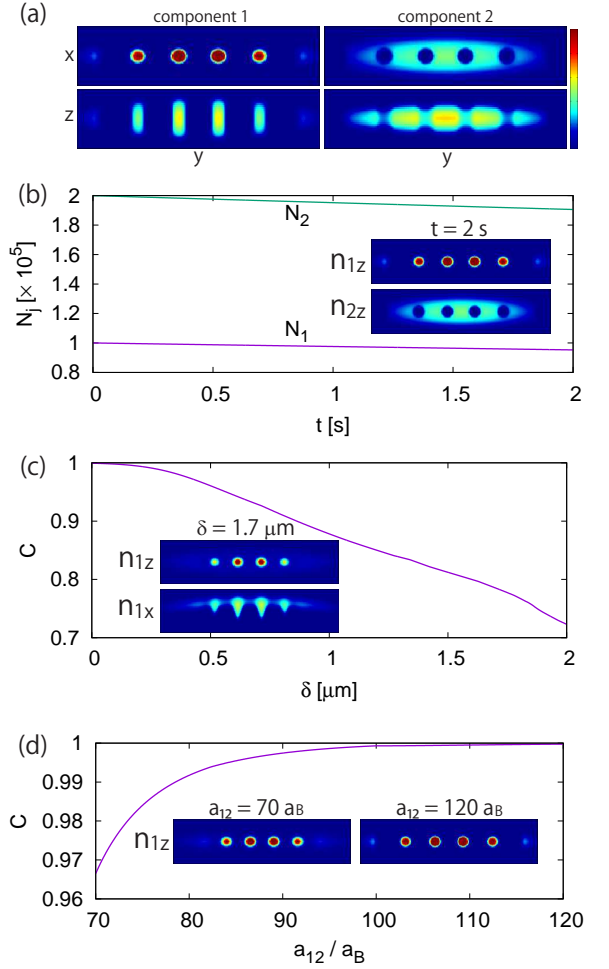


FIG. 1. (a) Integrated density distributions $n_{jz}(y, x) = \int dz |\psi_j(\mathbf{r})|^2$ and $n_{jx}(y, z) = \int dx |\psi_j(\mathbf{r})|^2$ of the ground state for $N_1 = 10^5$, $N_2 = 2 \times 10^5$, $a_{12} = 100a_B$, and $\delta = 0$. (b) Time evolution of the number N_j of atoms in component j with the three-body recombination loss, where the state in (a) is used as the initial state. The insets show $n_{1z}(y, x)$ and $n_{2z}(y, z)$ at $t = 2$ s. (c) Dependence of the contrast C on the sag δ . The insets show $n_{1z}(y, x)$ and $n_{1x}(y, z)$ for $\delta = 1.7 \mu\text{m}$. (d) Dependence of the contrast C on a_{12} . The insets show $n_{1z}(y, x)$ for $a_{12} = 70a_B$ and $120a_B$. In (c) and (d), other parameters are the same as those in (a). The images are $77\mu\text{m} \times 19.3\mu\text{m}$ in size. The color bar scales from 0 to $1.3 \times 10^3 \mu\text{m}^{-2}$.

the time step is $dt \simeq 10 \mu\text{s}$. To obtain the ground state, we solve the imaginary-time evolution. The intracomponent scattering lengths are fixed to $a_{11} = 83a_B$ [46] and $a_{22} = 100.4a_B$ [67], where a_B is the Bohr radius. The numbers of atoms are $N_1 = 10^5$ and $N_2 = 2 \times 10^5$.

First, we consider a system confined in a cigar-shaped trap with frequencies $\omega_{1x} = 2\pi \times 25$ Hz, $\omega_{1y} = 2\pi \times 5$ Hz, $\omega_{1z} = 2\pi \times 35$ Hz, and $\omega_{2x,y,z} = 1.8\omega_{1x,y,z}$. Figure 1(a) shows a typical droplet pattern formed in the two-component BEC. The erbium BEC splits into several droplets with a cylindrical shape, which align in the y di-

rection, and the rubidium BEC surrounds these droplets. We note that the droplets are stable without the LHY correction. In fact, the atomic density in each droplet is $\simeq 2 \times 10^{20} \text{ m}^{-3}$, which is smaller than that in the LHY droplet of ^{166}Er [44]. The three-body recombination loss is thus suppressed and the droplets can survive for longer time.

We confirm the long lifetime of the droplet lattice by simulating the real-time evolution including the atomic loss. The three-body recombination loss can be taken into account by adding the term $-i\hbar L_j^{(3)} |\psi_j|^4 \psi_j / 2$ to the right-hand side of Eq. (1). The loss rate $L_1^{(3)}$ for ^{166}Er largely depends on the scattering length near the Feshbach resonance, and for the present value of $a_{11} = 83a_B$, the loss rate is given by $L_1^{(3)} \simeq 2 \times 10^{-42} \text{ m}^6/\text{s}$ [44]. By contrast, in the experiment of LHY droplets, the scattering length must be smaller, where the loss rate is much larger (e.g., $L_1^{(3)} \simeq 6 \times 10^{-41} \text{ m}^6/\text{s}$ for $a_{11} \simeq 50a_B$ [44]). Thus, our system has an advantage not only of the low density but also of the small loss-rate coefficient, compared with the case of LHY droplets. The loss rate for ^{87}Rb is given by $L_2^{(3)} \simeq 5.8 \times 10^{-42} \text{ m}^6/\text{s}$ [68]. We neglect three-body processes in which both ^{166}Er and ^{87}Rb atoms participate, since the two components are almost separate from each other, as seen in Fig. 1 (a). Figure 1(b) shows the time evolution of the number of atoms N_j starting from the droplet lattice state in Fig. 1(a). The decay in the number of atoms is only a few percent for both components, and the droplet lattice is maintained even at $t = 2 \text{ s}$, indicating a much longer lifetime compared with the LHY droplets.

The appearance of a crystal-like structure by itself is not decisive evidence of a supersolid state. For supersolidity, the system must allow superflow between the droplets. A bottleneck for the superfluid current is caused by the density minimum along the pass between adjacent droplets. We therefore define the minimum density as $n_{\min} = \min_y [\max_{xz} |\psi_1(\mathbf{r})|^2]$, where the maximum in the x - z plane is taken first and the minimum along y between the droplets is chosen. The supersolidity can be quantified by the contrast C defined by

$$C = \frac{n_{\max} - n_{\min}}{n_{\max} + n_{\min}}, \quad (4)$$

where n_{\max} is the peak density of the droplets. The droplet lattice exhibits no supersolidity for $C = 1$, and the degree of supersolidity increases with decreasing C . The value of C for the state in Fig. 1(a) is larger than 0.99 and the degree of supersolidity is low.

To decrease the contrast C and enhance the supersolidity, we introduce a sag δ between the two components. Figure 1(c) shows C as a function of δ . We see that C decreases with δ , which indicates that the supersolidity is enhanced by the sag. This is because the droplets of component 1 are lifted upward for $\delta > 0$, and at the region near the upper edge, the adjacent droplets are strongly linked with each other, as seen in $n_{1x}(y, z)$ in

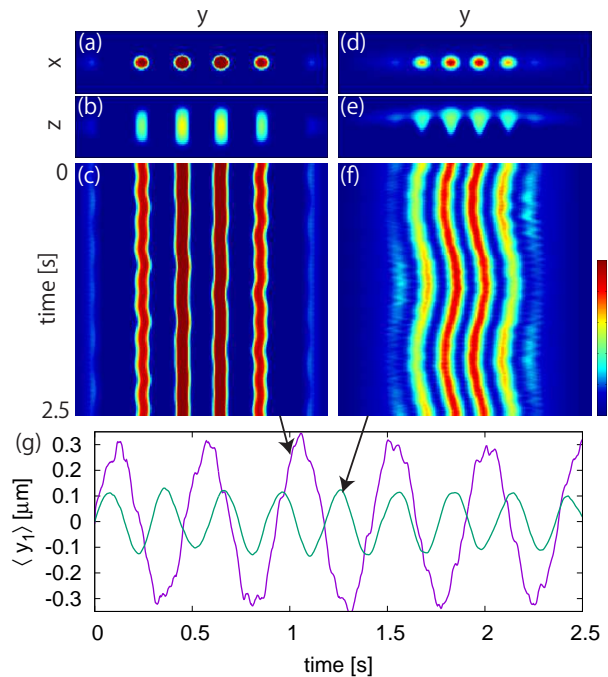


FIG. 2. Out-of-phase Goldstone mode in a one-dimensional supersolid. (a)-(c) Sag is absent, with $\delta = 0$ and (d)-(f) sag is present, with $\delta = 2.2 \mu\text{m}$. Integrated density profiles (a), (d) $n_{1z}(y, x) = \int dz |\psi_1(\mathbf{r})|^2$ and (b), (e) $n_{1x}(y, z) = \int dx |\psi_1(\mathbf{r})|^2$ of component 1 of the ground states, where the images are $77 \mu\text{m} \times 19.3 \mu\text{m}$. (c), (f) Time evolution of the integrated density profile $n_1(y, t) = \int dx dz |\psi_1(\mathbf{r}, t)|^2$ of component 1, where the three-body loss is included. The initial phase is imprinted as in Eq. (5) with $\phi = 0.2\pi$. The color bar scales from 0 to $1.3 \times 10^3 \mu\text{m}^{-2}$ for $n_{1z}(y, x)$ and $n_{1x}(y, z)$, and to $5.6 \times 10^3 \mu\text{m}^{-1}$ for $n_1(y, t)$. (g) Time evolution of the center-of-mass position of component 1 in the y direction, $\langle y_1(t) \rangle = \int d\mathbf{r} y |\psi_1(\mathbf{r}, t)|^2$, without and with sag. $\omega_{2x,y,z} = 1.6\omega_{1x,y,z}$ in (d)-(f). Other parameters are the same as those in Fig. 1(a).

Fig. 1(c). Thus, in the two-component system, the supersolidity can be controlled by the sag δ between the two components. When δ is larger, however, the number of droplets decreases and they disappear. In Fig. 1(c), the number of droplets changes to two for $\delta \gtrsim 1.8 \mu\text{m}$. Since the precise value of the intercomponent scattering length a_{12} between ^{166}Er and ^{87}Rb is unknown at present, we study the a_{12} dependence, which is shown in Fig. 1(d). The droplet pattern is stable for a wide range of a_{12} , and the present results are not very sensitive to the unknown parameter a_{12} . For $a_{12} \lesssim 65a_B$, the droplet pattern vanishes for the condition in Fig. 1(d).

Next, we investigate the dynamics of the droplets to examine the supersolidity. We imprint the initial phase to component 1 of the ground state ψ_1^{ground} as

$$\psi_1^{\text{initial}}(\mathbf{r}) = \begin{cases} \psi_1^{\text{ground}}(\mathbf{r}) e^{-i\phi} & (y < 0) \\ \psi_1^{\text{ground}}(\mathbf{r}) & (y \geq 0), \end{cases} \quad (5)$$

where we take $\phi = 0.2\pi$. The real-time evolution including the three-body loss is performed starting from this

initial state. Figures 2(a)-2(c) show the initial state and time evolution for $\delta = 0$. Since the initial phase $\phi > 0$ in Eq. (5) results in a positive phase gradient in the y direction, the system acquires a positive initial momentum, and the center-of-mass position $\langle y_1 \rangle$ first increases, followed by oscillation, as shown in Fig. 2(g). The amplitude $\simeq 0.3 \mu\text{m}$ is small, however, and the oscillation cannot be discerned in Fig. 2(c).

Figures 2(d)-2(f) show the case with $\delta = 2.2 \mu\text{m}$. As shown in Fig. 2(e), due to the sag, the droplets are connected to each other by nonzero density regions, which enhances the supersolidity. As a consequence, the dynamics shown in Fig. 2(f) is quite different from that in Fig. 2(c). Although the initial momentum given by the phase imprint is positive, the droplet pattern first moves to the negative direction (leftward). This counterintuitive motion is compensated by the superflow in the $+y$ direction, and in fact, $\langle y_1 \rangle$ first increases, followed by oscillation, as shown in Fig. 2(g). Its amplitude $\simeq 0.1 \mu\text{m}$ is much smaller than the apparent amplitude of the droplet lattice ($\simeq 2 \mu\text{m}$) in Fig. 2(f), which is due to the superflow opposite to the lattice movement. We can see in Fig. 2(f) that when the droplet lattice moves leftward (rightward), the density of the rightmost (leftmost) droplet increases due to the counter superflow, which is a hallmark of the out-of-phase Goldstone mode in a supersolid [9]. We note that such an out-of-phase Goldstone mode has a long period, which has hindered the direct observation of oscillation dynamics in experiments due to the short lifetime of the LHY droplets [9]. By contrast, the present two-component system has a long lifetime and allows the observation of long-time dynamics.

We move on to a two-dimensional supersolid produced in an oblate system. We consider a system confined in a trap with frequencies, $\omega_{1x} = \omega_{1y} = 2\pi \times 9 \text{ Hz}$, $\omega_{1z} = 66 \text{ Hz}$, and $\omega_{2x,y,z} = 1.5\omega_{1x,y,z}$. Figure 3(a) shows the ground state without sag ($\delta = 0$). The column densities integrated in the z direction clearly show a triangular lattice of erbium droplets surrounded by the rubidium condensate.

To study the supersolidity, we rotate the system about the z axis and calculate the moment of inertia Θ_j . We add a term $-\Omega L_z \psi_j$ to the right-hand side of Eq. (1) with a small Ω and solve the imaginary-time evolution to obtain the ground state in the rotating frame, where Ω is the rotation frequency of the system and $L_z = -i\hbar(x\partial_y - y\partial_x)$ is the angular momentum operator in the z direction. The moment of inertia for component j is defined as $\Theta_j = \lim_{\Omega \rightarrow 0} \int d\mathbf{r} \psi_j^*(\mathbf{r}) L_z \psi_j(\mathbf{r}) / \Omega$. To quantify the supersolidity, we normalize Θ_j by the moment of inertia for rigid-body rotation, $\Theta_j^{\text{rig}} = \int d\mathbf{r} (x^2 + y^2) |\psi_j(\mathbf{r})|^2$, and thus $\Theta_j / \Theta_j^{\text{rig}}$ can be regarded as the fraction of the classical moment of inertia. The quantity $\Theta_j / \Theta_j^{\text{rig}}$ vanishes for an isotropic state without droplets, and increases when droplets are formed [24, 34].

We change the sag δ and calculate $\Theta_j / \Theta_j^{\text{rig}}$ for the stationary state for each δ , which is shown in Fig. 3(b).

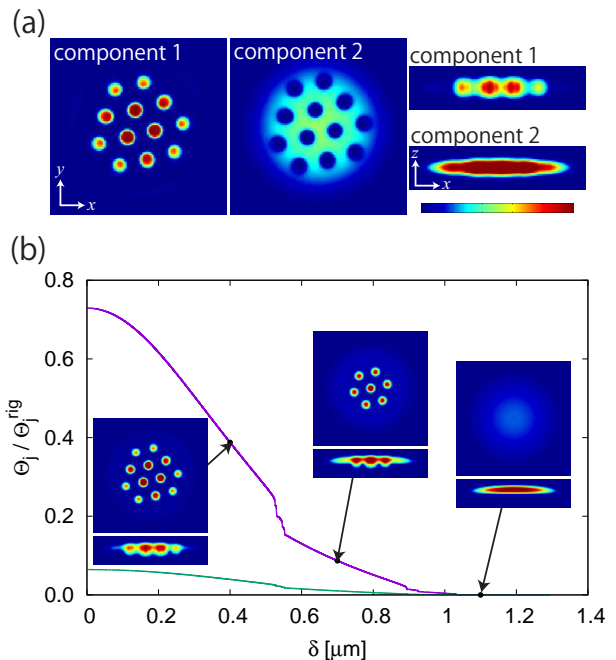


FIG. 3. Two-dimensional supersolid in an oblate trap for $a_{12} = 100a_B$. (a) Integrated density profiles $n_{jz}(x, y) = \int dz |\psi_j(\mathbf{r})|^2$ and $n_{jy}(x, z) = \int dy |\psi_j(\mathbf{r})|^2$ of components 1 and 2. (b) Normalized moment of inertia $\Theta_j / \Theta_j^{\text{rig}}$ as a function of the sag δ . The insets show $n_{1z}(x, y)$ and $n_{2y}(x, z)$. The sizes of the images are $55.2\mu\text{m} \times 55.2\mu\text{m}$ for $n_{jz}(x, y)$ and $55.2\mu\text{m} \times 13.8\mu\text{m}$ for $n_{jy}(x, z)$. The color bar scales from 0 to $6.4 \times 10^2 \mu\text{m}^{-2}$ for $n_{jz}(x, y)$ and to $1.1 \times 10^3 \mu\text{m}^{-2}$ for $n_{jy}(x, z)$.

When $\delta = 0$, the droplets are almost isolated from each other, and they behave as a classical crystal, giving the largest $\Theta_1 / \Theta_1^{\text{rig}} \simeq 0.7$. This is still smaller than unity due to the existence of the superfluid halo around the droplets [21]. The moment of inertia for component 2 is much smaller than that for component 1, since the porous pattern, as shown by $n_{2z}(x, y)$ in Fig. 3(a), does not much prevent superflow and the nonclassical nature is maintained. As the sag δ is increased, the droplet pattern is unchanged up to $\delta \simeq 0.5 \mu\text{m}$, while $\Theta_1 / \Theta_1^{\text{rig}}$ decreases to $\simeq 0.3$. This indicates that the Josephson links between the droplets are increased by the sag, in a manner similar to Fig. 2(e), and hence the supersolidity is enhanced. When δ is further increased, the number of droplets decreases and eventually the isotropic state without droplets with $\Theta_1 = 0$ is reached.

In conclusion, we have proposed a two-component BEC of a ^{166}Er - ^{87}Rb mixture to study supersolidity, where the LHY correction and the Feshbach control are not needed for the formation and stabilization of the droplet lattice state. The lifetime of the system is thus prolonged significantly, which enables us to observe long-time dynamics, such as an out-of-phase Goldstone mode. The coherence between droplets can be controlled by the difference δ between the trap centers of the two components.

The present results may also be realized by europium atoms [69] having the same magnetic moment as erbium.

This work was supported by JSPS KAKENHI Grant Number JP20K03804.

-
- [1] A. F. Andreev and I. M. Lifshits, Quantum theory of defects in crystals, *Sov. Phys. JETP* **29**, 1107 (1969).
- [2] A. J. Leggett, Can a solid be "superfluid"?, *Phys. Rev. Lett.* **25**, 1543 (1970).
- [3] J. Léonard, A. Morales, P. Zupancic, T. Esslinger, and T. Donner, Supersolid formation in a quantum gas breaking a continuous translational symmetry, *Nature* **543**, 87 (2017).
- [4] J.-R. Li, J. Lee, W. Huang, S. Burchesky, B. Shteynas, F. Ç. Top, A. O. Jamison, and W. Ketterle, A stripe phase with supersolid properties in spin-orbit-coupled Bose-Einstein condensates, *Nature* **543**, 91 (2017).
- [5] L. Tanzi, E. Lucioni, F. Famà, J. Catani, A. Fioretti, C. Gabbanini, R. N. Bisset, L. Santos, and G. Modugno, Observation of a dipolar quantum gas with metastable supersolid properties, *Phys. Rev. Lett.* **122**, 130405 (2019).
- [6] F. Böttcher, J.-N. Schmidt, M. Wenzel, J. Hertkorn, M. Guo, T. Langen, and T. Pfau, Transient supersolid properties in an array of dipolar quantum droplets, *Phys. Rev. X* **9**, 011051 (2019).
- [7] F. Böttcher, M. Wenzel, J.-N. Schmidt, M. Guo, T. Langen, I. Ferrier-Barbut, T. Pfau, R. Bombín, J. Sánchez-Baena, J. Boronat, and F. Mazzanti, Dilute dipolar quantum droplets beyond the extended Gross-Pitaevskii equation, *Phys. Rev. Research* **1**, 033088 (2019).
- [8] L. Tanzi, S. M. Roccuzzo, E. Lucioni, F. Famà, A. Fioretti, C. Gabbanini, G. Modugno, A. Recati, and S. Stringari, Supersolid symmetry breaking from compressional oscillations in a dipolar quantum gas, *Nature* **574**, 382 (2019).
- [9] M. Guo, F. Böttcher, J. Hertkorn, J.-N. Schmidt, M. Wenzel, H. P. Büchler, T. Langen, and T. Pfau, The low-energy Goldstone mode in a trapped dipolar supersolid, *Nature* **574**, 386 (2019).
- [10] G. Natale, R. M. W. van Bijnen, A. Patscheider, D. Petter, M. J. Mark, L. Chomaz, and F. Ferlaino, Excitation spectrum of a trapped dipolar supersolid and its experimental evidence, *Phys. Rev. Lett.* **123**, 050402 (2019).
- [11] J. Hertkorn, F. Böttcher, M. Guo, J. N. Schmidt, T. Langen, H. P. Büchler, and T. Pfau, Fate of the amplitude mode in a trapped dipolar supersolid, *Phys. Rev. Lett.* **123**, 193002 (2019).
- [12] L. Chomaz, D. Petter, P. Ilzhöfer, G. Natale, A. Trautmann, C. Politi, G. Durastante, R. M. W. van Bijnen, A. Patscheider, M. Sohmen, M. J. Mark, and F. Ferlaino, Long-lived and transient supersolid behaviors in dipolar quantum gases, *Phys. Rev. X* **9**, 021012 (2019).
- [13] M. A. Norcia, C. Politi, L. Klaus, E. Poli, M. Sohmen, M. J. Mark, R. N. Bisset, L. Santos, and F. Ferlaino, Two-dimensional supersolidity in a dipolar quantum gas, *Nature* **596**, 357 (2021).
- [14] L. Tanzi, J. G. Maloberti, G. Biagioni, A. Fioretti, C. Gabbanini, and G. Modugno, Evidence of superfluidity in a dipolar supersolid from nonclassical rotational inertia, *Science* **371**, 1162 (2021).
- [15] P. Ilzhöfer, M. Sohmen, G. Durastante, C. Politi, A. Trautmann, G. Natale, G. Morpurgo, T. Giamarchi, L. Chomaz, M. J. Mark, and F. Ferlaino, Phase coherence in out-of-equilibrium supersolid states of ultracold dipolar atoms, *Nat. Phys.* **17**, 356 (2021).
- [16] M. Sohmen, C. Politi, L. Klaus, L. Chomaz, M. J. Mark, M. A. Norcia, and F. Ferlaino, Birth, life, and death of a dipolar supersolid, *Phys. Rev. Lett.* **126**, 233401 (2021).
- [17] J. Hertkorn, J.-N. Schmidt, M. Guo, F. Böttcher, K. S. H. Ng, S. D. Graham, P. Uerlings, H. P. Büchler, T. Langen, M. Zwierlein, and T. Pfau, Supersolidity in two-dimensional trapped dipolar droplet arrays, *Phys. Rev. Lett.* **127**, 155301 (2021).
- [18] J. Hertkorn, J.-N. Schmidt, F. Böttcher, M. Guo, M. Schmidt, K. S. H. Ng, S. D. Graham, H. P. Büchler, T. Langen, M. Zwierlein, and T. Pfau, Density fluctuations across the superfluid-supersolid phase transition in a dipolar quantum gas, *Phys. Rev. X* **11**, 011037 (2021).
- [19] D. Petter, A. Patscheider, G. Natale, M. J. Mark, M. A. Baranov, R. van Bijnen, S. M. Roccuzzo, A. Recati, B. Blakie, D. Baillie, L. Chomaz, and F. Ferlaino, Bragg scattering of an ultracold dipolar gas across the phase transition from Bose-Einstein condensate to supersolid in the free-particle regime, *Phys. Rev. A* **104**, L011302 (2021).
- [20] H. Kadau, M. Schmitt, M. Wenzel, C. Wink, T. Maier, I. Ferrier-Barbut, and T. Pfau, Observing the Rosensweig instability of a quantum ferrofluid, *Nature* **530**, 194 (2016).
- [21] D. Baillie and P. B. Blakie, Droplet crystal ground states of a dipolar Bose gas, *Phys. Rev. Lett.* **121**, 195301 (2018).
- [22] Y.-C. Zhang, F. Maucher, and T. Pohl, Supersolidity around a critical point in dipolar Bose-Einstein condensates, *Phys. Rev. Lett.* **123**, 015301 (2019).
- [23] S. M. Roccuzzo and F. Ancilotto, Supersolid behavior of a dipolar Bose-Einstein condensate confined in a tube, *Phys. Rev. A* **99**, 041601 (2019).
- [24] S. M. Roccuzzo, A. Gallemí, A. Recati, and S. Stringari, Rotating a supersolid dipolar gas, *Phys. Rev. Lett.* **124**, 045702 (2020).
- [25] A. Gallemí, S. M. Roccuzzo, S. Stringari, and A. Recati, Quantized vortices in dipolar supersolid Bose-Einstein condensed gases, *Phys. Rev. A* **102**, 023322 (2020).
- [26] P. B. Blakie, D. Baillie, L. Chomaz, and F. Ferlaino, Supersolidity in an elongated dipolar condensate, *Phys. Rev. Research* **2**, 043318 (2020).
- [27] M. N. Tengstrand, D. Boholm, R. Sachdeva, J. Bengtsson, and S. M. Reimann, Persistent currents in toroidal dipolar supersolids, *Phys. Rev. A* **103**, 013313 (2021).
- [28] F. Ancilotto, M. Barranco, M. Pi, and L. Reatto, Vortex properties in the extended supersolid phase of dipolar Bose-Einstein condensates, *Phys. Rev. A* **103**, 033314 (2021).
- [29] Y.-C. Zhang, T. Pohl, and F. Maucher, Phases of supersolids in confined dipolar Bose-Einstein condensates, *Phys. Rev. A* **104**, 013310 (2021).
- [30] E. Poli, T. Bland, C. Politi, L. Klaus, M. A.

- Norcia, F. Ferlaino, R. N. Bisset, and L. Santos, Maintaining supersolidity in one and two dimensions, *Phys. Rev. A* **104**, 063307 (2021).
- [31] J. Hertkorn, J.-N. Schmidt, M. Guo, F. Böttcher, K. S. H. Ng, S. D. Graham, P. Uerlings, T. Langen, M. Zwerlein, and T. Pfau, Pattern formation in quantum ferrofluids: From supersolids to superglasses, *Phys. Rev. Research* **3**, 033125 (2021).
- [32] B. K. Turmanov, B. B. Baizakov, F. K. Abdullaev, and M. Salerno, Oscillations of a quasi-one-dimensional dipolar supersolid, *J. Phys. B: At. Mol. Opt. Phys.* **54**, 145302 (2021).
- [33] S. Pal, D. Baillie, and P. B. Blakie, Infinite dipolar droplet: A simple theory for the macrodroplet regime, *Phys. Rev. A* **105**, 023308 (2022).
- [34] S. M. Rocuzzo, A. Recati, and S. Stringari, Moment of inertia and dynamical rotational response of a supersolid dipolar gas, *Phys. Rev. A* **105**, 023316 (2022).
- [35] S. M. Rocuzzo, S. Stringari, and A. Recati, Supersolid edge and bulk phases of a dipolar quantum gas in a box, *Phys. Rev. Research* **4**, 013086 (2022).
- [36] K.-T. Xi and H. Saito, Droplet formation in a Bose-Einstein condensate with strong dipole-dipole interaction, *Phys. Rev. A* **93**, 011604(R) (2016).
- [37] R. N. Bisset and P. B. Blakie, Crystallization of a dilute atomic dipolar condensate, *Phys. Rev. A* **92**, 061603(R) (2015).
- [38] T. D. Lee, K. Huang, and C. N. Yang, Eigenvalues and eigenfunctions of a Bose system of hard spheres and its low-temperature properties, *Phys. Rev.* **106**, 1135 (1957).
- [39] F. Wächtler and L. Santos, Quantum filaments in dipolar Bose-Einstein condensates, *Phys. Rev. A* **93**, 061603(R) (2016).
- [40] F. Wächtler and L. Santos, Ground-state properties and elementary excitations of quantum droplets in dipolar Bose-Einstein condensates, *Phys. Rev. A* **94**, 043618 (2016).
- [41] I. Ferrier-Barbut, H. Kadau, M. Schmitt, M. Wenzel, and T. Pfau, Observation of quantum droplets in a strongly dipolar Bose gas, *Phys. Rev. Lett.* **116**, 215301 (2016).
- [42] H. Saito, Path-integral Monte Carlo study on a droplet of a dipolar Bose-Einstein condensate stabilized by quantum fluctuation, *J. Phys. Soc. Jpn.* **85**, 053001 (2016).
- [43] M. Schmitt, M. Wenzel, F. Böttcher, I. Ferrier-Barbut, and T. Pfau, Self-bound droplets of a dilute magnetic quantum liquid, *Nature* **539**, 259 (2016).
- [44] L. Chomaz, S. Baier, D. Petter, M. J. Mark, F. Wächtler, L. Santos, and F. Ferlaino, Quantum-fluctuation-driven crossover from a dilute Bose-Einstein condensate to a macrodroplet in a dipolar quantum fluid, *Phys. Rev. X* **6**, 041039 (2016).
- [45] A. Trautmann, P. Ilzhöfer, G. Durastante, C. Politi, M. Sohmen, M. J. Mark, and F. Ferlaino, Dipolar quantum mixtures of erbium and dysprosium atoms, *Phys. Rev. Lett.* **121**, 213601 (2018).
- [46] C. Politi, A. Trautmann, P. Ilzhöfer, G. Durastante, M. J. Mark, M. Modugno, and F. Ferlaino, Interspecies interactions in an ultracold dipolar mixture, *Phys. Rev. A* **105**, 023304 (2022).
- [47] K. Góral and L. Santos, Ground state and elementary excitations of single and binary Bose-Einstein condensates of trapped dipolar gases, *Phys. Rev. A* **66**, 023613 (2002).
- [48] H. Saito, Y. Kawaguchi, and M. Ueda, Ferrofluidity in a two-component dipolar Bose-Einstein condensate, *Phys. Rev. Lett.* **102**, 230403 (2009).
- [49] G. Gligorić, A. Maluckov, M. Stepić, L. c. v. Hadžievski, and B. A. Malomed, Transition to miscibility in linearly coupled binary dipolar Bose-Einstein condensates, *Phys. Rev. A* **82**, 033624 (2010).
- [50] P. Jain and M. Boninsegni, Quantum demixing in binary mixtures of dipolar bosons, *Phys. Rev. A* **83**, 023602 (2011).
- [51] K.-T. Xi, J. Li, and D.-N. Shi, Phase separation of a two-component dipolar Bose-Einstein condensate in the quasi-one-dimensional and quasi-two-dimensional regime, *Phys. Rev. A* **84**, 013619 (2011).
- [52] L. E. Young-S. and S. K. Adhikari, Mixing, demixing, and structure formation in a binary dipolar Bose-Einstein condensate, *Phys. Rev. A* **86**, 063611 (2012).
- [53] R. M. Wilson, C. Ticknor, J. L. Bohn, and E. Timmermans, Roton immiscibility in a two-component dipolar Bose gas, *Phys. Rev. A* **86**, 033606 (2012).
- [54] L. E. Young-S. and S. K. Adhikari, Dipolar droplet bound in a trapped Bose-Einstein condensate, *Phys. Rev. A* **87**, 013618 (2013).
- [55] Y. Zhao, J. An, and C.-D. Gong, Vortex competition in a rotating two-component dipolar Bose-Einstein condensate, *Phys. Rev. A* **87**, 013605 (2013).
- [56] S. K. Adhikari, Demixing and symmetry breaking in binary dipolar Bose-Einstein-condensate solitons, *Phys. Rev. A* **89**, 013630 (2014).
- [57] X.-F. Zhang, L. Wen, C.-Q. Dai, R.-F. Dong, H.-F. Jiang, H. Chang, and S.-G. Zhang, Exotic vortex lattices in a rotating binary dipolar Bose-Einstein condensate, *Sci. Rep.* **6**, 1 (2016).
- [58] R. K. Kumar, L. Tomio, B. A. Malomed, and A. Gammal, Vortex lattices in binary Bose-Einstein condensates with dipole-dipole interactions, *Phys. Rev. A* **96**, 063624 (2017).
- [59] V. Pastukhov, Beyond mean-field properties of binary dipolar Bose mixtures at low temperatures, *Phys. Rev. A* **95**, 023614 (2017).
- [60] K.-T. Xi, T. Byrnes, and H. Saito, Fingering instabilities and pattern formation in a two-component dipolar Bose-Einstein condensate, *Phys. Rev. A* **97**, 023625 (2018).
- [61] R. K. Kumar, L. Tomio, and A. Gammal, Spatial separation of rotating binary Bose-Einstein condensates by tuning the dipolar interactions, *Phys. Rev. A* **99**, 043606 (2019).
- [62] A.-C. Lee, D. Baillie, P. B. Blakie, and R. N. Bisset, Miscibility and stability of dipolar bosonic mixtures, *Phys. Rev. A* **103**, 063301 (2021).
- [63] R. N. Bisset, L. A. Peña Ardila, and L. Santos, Quantum droplets of dipolar mixtures, *Phys. Rev. Lett.* **126**, 025301 (2021).
- [64] J. C. Smith, D. Baillie, and P. B. Blakie, Quantum droplet states of a binary magnetic gas, *Phys. Rev. Lett.* **126**, 025302 (2021).
- [65] D. Scheiermann, L. A. P. Ardila, T. Bland, R. N. Bisset, and L. Santos, Catalyzation of supersolidity in binary dipolar condensates (2022), arXiv:2202.08259 [cond-mat.quant-gas].
- [66] Here we ignore the LHY term. We have numerically confirmed that our results are almost unchanged even in the presence of the LHY term.
- [67] E. G. M. van Kempen, S. J. J. M. F. Kokkelmans, D. J.

- Heinzen, and B. J. Verhaar, Interisotope determination of ultracold rubidium interactions from three high-precision experiments, *Phys. Rev. Lett.* **88**, 093201 (2002).
- [68] E. A. Burt, R. W. Ghrist, C. J. Myatt, M. J. Holland, E. A. Cornell, and C. E. Wieman, Coherence, correlations, and collisions: What one learns about Bose-Einstein condensates from their decay, *Phys. Rev. Lett.* **79**, 337 (1997).
- [69] Y. Miyazawa, R. Inoue, H. Matsui, K. Takanashi, and M. Kozuma, Narrow-line magneto-optical trap for europium, *Phys. Rev. A* **103**, 053122 (2021).